Measurement of the optical phase statistics of single-mode semiconductor lasers biased around the threshold current

A. VALLE,[1,*] ⓘ A. ROSADO,[2,3,4] G. SOLDEVILLA,[2] AND I. ESQUIVIAS[2]

[1]*Instituto de Física de Cantabria (CSIC-Univ. Cantabria), Avda. Los Castros s/n, E39005 Santander, Spain*
[2]*CEMDATIC- E.T.S.I. Telecomunicación, Universidad Politécnica de Madrid (UPM), 28040 Madrid, Spain*
[3]*Photonics Systems and Sensing Lab, School of Electronic Engineering, Dublin City University, Glasnevin, Dublin 9, Ireland*
[4]*CONNECT Centre, Trinity College Dublin, D02 W272 Dublin, Ireland*
*valle@ifca.unican.es

Abstract: We report on the experimental analysis of the statistics of the optical phase of the light emitted by a distributed-feedback (DFB) laser. We measure the dependence of the phase diffusion coefficient on the applied bias current in the region around the threshold current. We measure the phase noise statistics using three different methods based on i) averages of the noise phase trajectories over different temporal windows, ii) the variance of the phase noise difference, and iii) the frequency noise spectral density. The comparison between the results obtained with these methods is succesful. We obtain that the phase diffusion coefficient monotonously decreases with the bias current in the region around threshold. We finally compare our experimental results with simple analytical expressions for the below and above threshold cases based on Schawlow–Townes laws.

1. Introduction

The study of semiconductor laser phase fluctuations is relevant in quantum communications since many quantum random number generation (QRNG) [1–4] and quantum key distribution (QKD) [5–7] systems are based on those fluctuations. QRNGs are random number generators that utilize the intrinsic randomness of fundamental quantum processes to generate completely unpredictable random numbers. QRNGs find applications in many fields like cryptography, computer simulation, lotteries, fundamental physics test, data processing, industrial testing, etc [1–4]. QRNGs have been demonstrated with different optical systems such as single photons [8,9], optical vacuum states [10,11], and phase fluctuations from a semiconductor laser [12–25]. The laser phase noise originates from spontaneous emission that is quantum mechanical in origin [26,27].

Two types of phase noise QRNGs can be distinguished. In the first one, the laser operates in cw mode with a constant applied bias current above the threshold value [12–16]. Unbalanced Mach-Zehnder interferometers [12,13,16], or optical hybrids feed with one [15] or two independent laser sources [14] have been used to measure the random phase fluctuations induced by spontaneous emission noise, from which the random numbers are obtained. In the second type, the laser diode is gain-switched from below to above the threshold current in order to generate trains of pulses with random phases [17–25]. During the below threshold operation the optical phase becomes random, faster than in the above threshold operation, due to the predominance of amplified spontaneous emission in the below threshold regime. Phase fluctuations are converted into amplitude fluctuations by using an unbalanced Mach-Zehnder interferometer with a delay matching the pulse repetition period. The amplitude values, measured with a photodetector,

are postprocessed to provide the random numbers. This type of QRNG has the advantage of generating samples that follow an arcsine distribution that is markedly distinct from that of the electronic noise [18]. Both types of QRNGs have the advantages of being fast, robust, and low-cost. Also both types of QRNGs can be integrated in photonic integrated circuits [13,16,20,23–25]. Since in both types of QRNGs the randomness of the optical phase is the basis of the generators, the statistical characterization of phase fluctuations is a problem worth studying.

This characterization has been mainly performed when a single-frequency semiconductor laser is biased above its threshold current because a high degree of temporal coherence is required in applications like coherent optical communications [28,29], fiber-optic sensing [30], or high-resolution spectroscopy [31]. For QRNG applications the analysis of phase noise for lasers biased below threshold also becomes of interest. The phase noise is characterised by a Gaussian statistics with zero average and a variance that increases linearly with time with a proportionality constant given by twice the phase diffusion coefficient [26,29,32–38]. This coefficient is also shown to be proportional to the lasing spectral linewidth [32,35–37]. We have recently performed direct phase measurements using a 90° optical hybrid in a cw-discrete mode laser (DML) for a current slightly below the threshold value showing a Gaussian statistics of the phase with a variance growing linearly in time [39]. This is in agreement with the diffusive behaviour of the optical phase obtained theoretically from first principles [26,33–38]. In the gain-switching regime some indirect measurements of phase fluctuations have been performed [21,22]. In [21] the distribution of intensities at the output of an asymmetric interferometer is measured to obtain the variance of the phase noise as the fitting parameter of that distribution. Also the standard deviation of the phase noise has been obtained from the visibility of the pulse interference fringes [22].

In this work we will focus on the measurement of the phase fluctuations in a single-mode laser diode. We will restrict to the simplest case of a laser operating in cw-mode. We will consider several methods for measuring the variance of the phase noise, going from the well established methods based on the average of the squared phase noise difference or the frequency noise spectral density [29,32], to the recently proposed based on averages over different phase noise trajectories [39]. Our measurements will focus on the dependence of the phase diffusion coefficient on the applied bias current in the region around the laser threshold. This experimental analysis has not been performed up to now to the best of our knowledge. We will show that there is a decreasing monotonic dependence of the diffusion coefficient on the applied bias current.

Our paper is organized as follows: in section 2, we present our experimental setup and characterization of the laser. Section 3 is devoted to explain the different methods that we have used for measuring the phase diffusion coefficient. Section 4 is devoted to show our experimental results. Finally, in section 5 we discuss and summarize our results.

2. Experimental setup and characterization of the distributed feedback laser

The experimental setup is shown in Fig. 1. A 1550 nm commercial distributed-feedback (DFB) laser (JDS Uniphase model CQF915/108) has been characterized. The light of this laser (denoted as SIG in Fig. 1) is launched through an optical isolator into the signal input of a dual-polarization coherent receiver (Finisar CPRV2222A, 25 GHz bandwidth). A low-linewidth tunable laser (Pure Photonics PPCL300, with measured linewidth of 75 kHz) is used as a local oscillator (LO), providing an optical power of $P_{LO} = -10$ dBm. At every DFB current the LO is slightly tuned to emit at the DFB wavelength, which is checked by measuring both spectra in a Brillouin optical spectrum analyzer (BOSA, Aragon Photonics model 400 C+L, 10 MHz resolution). At the input of the coherent receiver, the polarization of the LO is adjusted to maximize the electrical output of one of the polarizations. The n-and p- output voltages corresponding to the in-phase and quadrature components are combined by means of two different baluns (Marki Microwave

BALH0010, bandwidth of 200kHz to 10 GHz) and are digitized by a real-time oscilloscope (denoted OSC in Fig. 1, Keysight MSOS804A, 8 GHz bandwidth). The electronic bandwidth in our measurement system is limited by our oscilloscope. We have checked that it is enough to capture the fast optical phase variations in the considered experimental conditions [40].
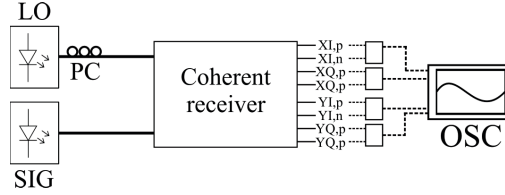

Fig. 1. Schematics of the experimental set-up. LO: local oscillator, SIG: laser signal; PC: polarization controller; OSC: oscilloscope.

The measurement of the threshold current of the laser, I_{th}, is performed by using the method of Refs. [41,42]. In summary, when the current, I, is close to I_{th}, the optical power around the lasing frequency, P, can be written as

$$FP = \frac{1}{2}\left(I - I_{th} + \sqrt{(I - I_{th})^2 + C}\right),\tag{1}$$

where F is the scale factor between the value of P above threshold and the injected current, $P = (I - I_{th})/F$, C is a constant given by $C = 4e^2 R_{sp}^{th}/(\tau_n \tau_p G_N)$, e is the electron charge, R_{sp}^{th} is the spontaneous emission rate coupled to the laser mode at threshold, τ_n is the differential carrier lifetime at threshold, τ_p is the photon lifetime, and G_N is the differential gain [42].
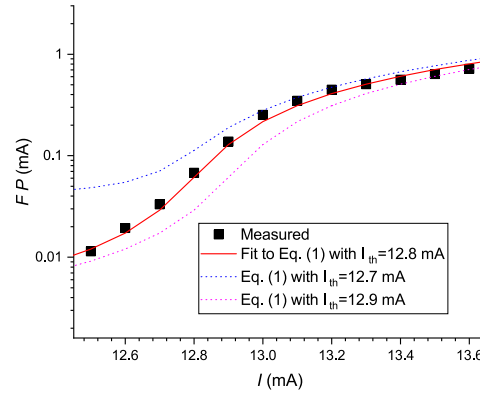

Fig. 2. Measured FP as a function of the bias current. Experimental data are plotted with squares. The best fit to Eq. (1) is plotted with solid line. Results obtained with Eq. (1) for another two values of I_{th} are also plotted with dotted and dashed lines.

We have measured P as a function of I with the BOSA using a 10 GHz span. A linear relation is found between P and I above 12.8 mA, that is our first estimation of I_{th}. By linearly fitting the points above that estimation to $P = (I - I_{th})/F$ we obtain that $F = 2.62$ mA/mW. We can now represent FP as a function of I and use Eq. (1) to calculate I_{th} and C. We show in Fig. 2 with symbols the experimental values of FP in a logarithmic scale when I is around threshold. Using a fitting procedure similar to that in [42] we obtain the best fit for $I_{th} = 12.80 \pm 0.02$ mA and $C = 0.015 \pm 0.05$ mA^2. This fit, also shown in Fig. 2 with a solid line, agrees well with the experimental values. We also show in that figure the results obtained with Eq. (1) using two values for I_{th} out of the estimated range.

3. Evaluation methods of phase noise statistics

We now explain the three methods that we have used to measure the phase noise statistics. We depart from the expressions of the electrical field corresponding to the DFB and the local oscillator, $S(t) = A_s \exp[i(\omega_s t + \varphi(t))]$, $LO(t) = A_{LO} \exp[i\omega_{LO}t]$, where A_s and A_{LO} are the corresponding amplitudes. ω_s and ω_{LO} are the angular optical frequencies of the DFB and the LO, and $\varphi(t)$ is the phase noise of the DFB. We have considered that the strength of the phase noise of the LO is much smaller than that of the DFB, a condition that is fulfilled for the values of the current that we apply to the DFB, around I_{th}. Outputs at photodetectors 1 and 2, $V_I(t)$ and $V_Q(t)$, are proportional to $\frac{1}{\sqrt{2}}A_s A_{LO} \sin[\theta(t)]$, and $\frac{1}{\sqrt{2}}A_s A_{LO} \cos[\theta(t)]$, respectively, where $\theta(t) = \Delta\omega t + \varphi(t)$, and $\Delta\omega = (\omega_s - \omega_{LO})$.

The first method, detailed in [39], calculates $\theta(t)$ from $V_I(t)$ and $V_Q(t)$. $\theta(t)$ is calculated from $\theta(t) = \arctan(V_I/V_Q)$ that gives results between $-\pi/2$ and $\pi/2$. These results are then processed with the algorithm detailed in the Appendix B of [43] to obtain a continuous and unbounded value of $\theta(t)$. Alternatively, the arctan2 function can be used to obtain wrapped phases between $-\pi$ and π that can be processed with a phase unwrapping algorithm, like unwrap (Matlab or Python), to obtain the unbounded and continuous $\theta(t)$ within the temporal window.

A long sequence of data is divided in windows of duration T_w. Phase noise is then obtained for each window from $\varphi(t) = \theta(t) - \Delta\omega t$ by assuming that $\Delta\omega$ remains constant over that window. Since fluctuations of the laser instantaneous frequencies on long time scales are large [44] measurements with small values of T_w must be performed so that $\Delta\omega$ can be considered as approximately constant in each window. The value of $\Delta\omega$ for each temporal window is calculated as $\Delta\omega = \overline{\frac{d\theta}{dt}}$ where $\overline{\frac{d\theta}{dt}}$ is the temporal average of $\frac{d\theta}{dt}$ over a window of duration T_w [39]. Each window is divided in j equal intervals, $T_w = j\Delta t$, where Δt is the sampling time. $\frac{d\theta}{dt}$ is calculated by discretising the derivative $\frac{d\theta}{dt}\big]_{t_i} = (\theta(t_{i+1}) - \theta(t_i))/\Delta t$, where $t_i = i\Delta t$, and $i = 0, \ldots, j - 1$. The temporal average of this derivative is calculated in the following way:

$$\overline{\frac{d\theta}{dt}} = \frac{1}{j}\sum_{i=0}^{j-1} \frac{d\theta}{dt}\bigg]_{t_i} = \frac{\theta(T_w) - \theta(0)}{T_w} = \Delta\omega, \tag{2}$$

and $\varphi(t_i) = \theta(t_i) - \Delta\omega t_i$. Statistical moments of $\varphi(t)$ are denoted as $\langle\varphi^n(t)\rangle$, where the angled brackets mean an average over different windows. In these averages we have considered that the initial value in each window, $\varphi(0)$, corresponds to the value at the end of the previous window but converted into the $[-\pi, \pi)$ interval. The phase diffusion coefficient, D_φ, is defined from $\sigma_\varphi^2(t) = 2D_\varphi t$, where $\sigma_\varphi^2(t) = \langle\varphi^2\rangle - \langle\varphi\rangle^2$. In this method D_φ is calculated from the linear fitting of $\sigma_\varphi^2(t)$ versus t for small values of t.

The second method [29,32,35] is based on the analysis of the difference in phase fluctuations at times t and $t + \tau$, $\Delta\varphi_\tau(t) = \varphi(t + \tau) - \varphi(t)$, that is a stationary random process. For each value of τ, the variance of the phase noise, $\sigma_\varphi^2(\tau) = \langle\Delta\varphi_\tau^2(t)\rangle$ does not depends on t because $\Delta\varphi_\tau(t)$ is stationary, and therefore it can be calculated from the temporal average $\sigma_\varphi^2(\tau) = \overline{\Delta\varphi_\tau^2(t)}$. We calculate this quantity in the following way:

$$\overline{\Delta\varphi_\tau^2(t)} = \frac{1}{j - \text{int}(\tau/\Delta t) + 1} \sum_{i=0}^{j-\text{int}(\tau/\Delta t)} (\varphi(t_i + \tau) - \varphi(t_i))^2. \tag{3}$$

We consider the upper limit in the summatory, $j - \text{int}(\tau/\Delta t)$, in order to have all the evaluated values of φ inside the window. For each value of τ we calculate this sum, so $\sigma_\varphi^2 = \overline{\Delta\varphi_\tau^2(t)}$ is a function of τ. The phase diffusion coefficient obtained with the second method, D_τ, is obtained from $\sigma_\varphi^2(\tau) = 2D_\tau\tau$, that again is calculated from the linear fitting of $\sigma_\varphi^2(\tau)$ versus τ for small

values of τ. A good agreement between the values of D_φ and D_τ was found in [39] for a value of the bias current below threshold.

The third method [29,32] relies on the calculation of the FM-noise spectrum, $S_F(f)$, defined as the power spectral density function of the instantaneous frequency fluctuations. It can be calculated from the Fourier transform, $F(f)$, of the instantaneous frequency fluctuation, $\frac{1}{2\pi}\frac{d\varphi}{dt}$, by

$$S_F(f) = \lim_{T\to\infty} \frac{1}{T}\langle F^*(f)F(f)\rangle. \tag{4}$$

The instantaneous frequency fluctuation can be calculated from $\frac{1}{2\pi}\frac{d\varphi}{dt} = \frac{1}{2\pi}\left(\frac{d\theta}{dt} - \Delta\omega\right)$. In the ideal case of white FM noise its single-sided spectral density, $\mathbf{S_F}(f)$, defined as $\mathbf{S_F}(f) = 2S_F(f)$, $f \geq 0$, is constant and given by

$$\mathbf{S_F}(f) = \frac{D_F}{\pi^2}. \tag{5}$$

where $D_F = D_\tau$ when the bias current is above threshold [29,32].

In the next section we will use linear fits of $\sigma_\varphi^2(t)$, $\sigma_\varphi^2(\tau)$, and Eq. (5) to obtain D_φ, D_τ and D_F, respectively. In this way we will check if these values are similar, as obtained from the solution of the stochastic semiconductor laser rate equations [29,32,35].

4. Experimental results

In our experiments we have measured phase noise characteristics in a range of currents around I_{th} spanning from 12.3 mA to 13.9 mA. Figure 3(a) and Fig. 3(b) show the temporal evolution of phase noise for eight trajectories when the laser is biased below and above I_{th}, respectively. These trajectories are obtained from a long sequence of data (2 ms) that is divided in windows of duration $T_w = 1\mu s$ with a sampling rate of 2 GSa/s. In both figures a dispersion of the initial conditions is observed that corresponds to the way in which $\varphi(0)$ values have been chosen, as explained in the previous section. The typical Brownian broadening of the trajectories is observed during the initial stages of the evolution. The comparison between Fig. 3(a) and Fig. 3(b) shows a larger widening of the trajectories as the bias current decreases. We also check the assumption of constant $\Delta\omega$ during each temporal window for the cases shown in Fig. 3. In order to do this we have calculated $\Delta\omega/(2\pi)$ for each of 2000 windows. This quantity fluctuates around its averaged value, $\langle\Delta\omega/(2\pi)\rangle$=-9.0 MHz (-12.6 MHz), with a standard deviation of 19.8 MHz (4.6 MHz) when the bias current is 12.7 mA (13.2 mA).
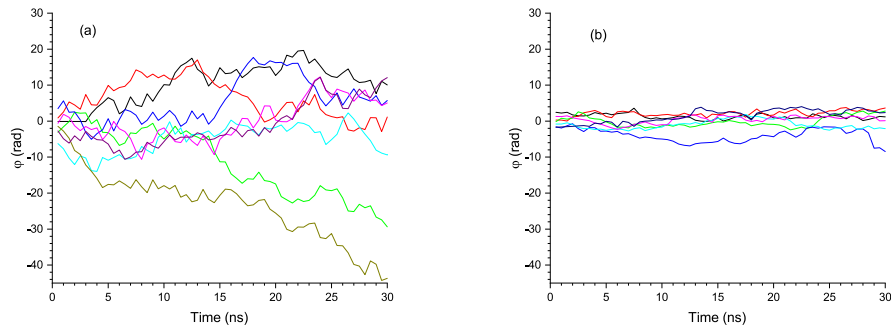

Fig. 3. Phase noise for different temporal trajectories for a bias current of (a) 12.7 mA, and (b) 13.2 mA. In this figure the sampling rate is 2 GSa/s and $T_w = 1\,\mu s$.

Let us now calculate the variance of the phase noise by using the first two methods, $\sigma_\varphi^2(t)$ and $\sigma_\varphi^2(\tau)$, as explained in the previous section. Figure 4 shows those quantities for two values of

the bias current in the initial stages of the evolution, in which a linear dependence on time is observed, as expected. The size of temporal windows is $T_w = 1\mu s$ and $T_w = 32.768\mu s$ for the first and two methods. A longer window is chosen for the second method for a more accurate calculation of the required temporal average, $\overline{\Delta\varphi_\tau^2(t)}$.
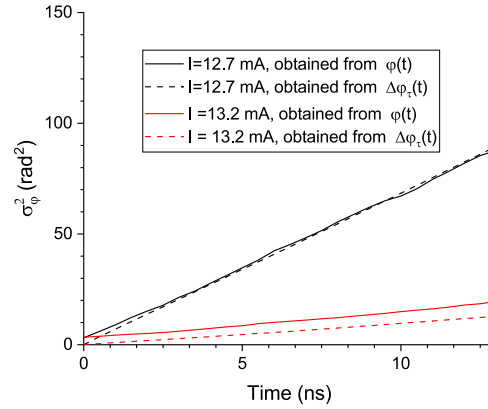

Fig. 4. Temporal evolution of the phase variance for short values of *t* for two values of the bias current, 12.7 and 13.2 mA.

The results obtained with both methods agree well when the current is below threshold. The linear fit of the points from 0 to 10 ns gives the following values of the phase diffusion coefficients: $D_\varphi = 3.37 \pm 0.02$ rad^2/ns ($D_\tau = 3.40 \pm 0.01$ rad^2/ns) for the first (second) method when $I = 12.7$ mA. For the case of $I = 13.2$ mA we obtain that the slopes are very similar, $D_\varphi = 0.43 \pm 0.01$ rad^2/ns ($D_\tau = 0.45 \pm 0.01$ rad^2/ns) for the first (second) method although the values are different. This is due to the nonzero value of the variance at $t = 0$ obtained with the first method in contrast to the zero value that is obtained with the second method when $\tau = 0$.

Figure 5 shows the one-sided spectral density of FM noise for four different values of the current, including the two previously analysed. Each spectrum is calculated by averaging one-sided spectra over 480 windows of 2.048 μs duration, with a 500 ps sampling time. As expected, there is a wide range of frequencies in which spectra are flat [29]. The phase diffusion coefficient, D_F, is obtained by using $D_F = \pi^2 \mathbf{S_F}$, where $\mathbf{S_F}$ is the averaged value of $\mathbf{S_F}(f)$ over the interval $(0.01, 0.8)$ GHz shown in Fig. 5. The values of D_F for $I = 12.7$ mA and $I = 13.2$ mA are 3.6 rad^2/ns and 0.52 rad^2/ns, respectively, that are close to those found with the first two methods. We note that a shallow resonance peak appears in the spectrum at 0.46 GHz when the current is 13.2 mA. This frequency corresponds to the relaxation oscillation frequency. A resonance peak in the FM-noise spectra appears at the relaxation oscillation frequency [28]. When the current is below the threshold value the peak does not appear. We have also checked that when the current increases (13.6 mA) the peak appears at a larger frequency (0.82 GHz) that corresponds to the relaxation oscillation frequency at that value of the current.

The dependence of the phase diffusion coefficient on the bias current in the region around the threshold value is shown in Fig. 6. This figure also shows the comparison between the results obtained with the three methods when the sampling rate is 2 GSa/s. We note that the values of D_τ have been obtained by averaging the values obtained with the method previously described over 30 windows. Similar results are obtained with the three methods. D_φ, D_τ and D_F monotonously increases as the bias current decreases until reaching $I = 12.8$ mA.

Below that current, saturation of the diffusion coefficients around a constant value is obtained. This saturation should not appear since further increase of the diffusion coefficient would be expected as the current decreases. The reason why this saturation appears is that the sampling
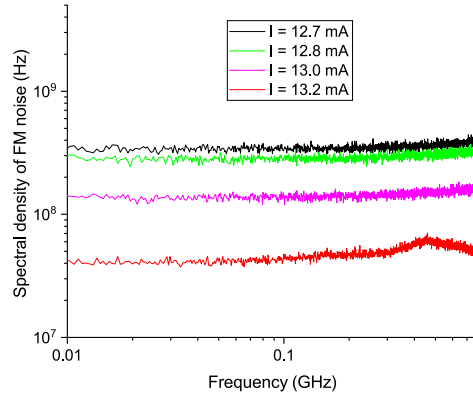
Fig. 5. Single-sided FM-noise spectrum for several values of the bias current. The sampling rate is 2 GSa/s.
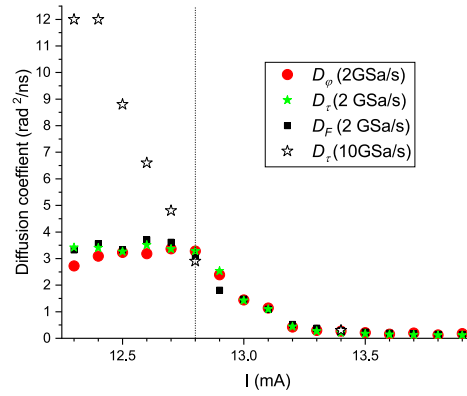

Fig. 6. Phase diffusion coefficients obtained with different methods as a function of the bias current. Results for a sampling rate of 2 GSa/s (10 GSa/s) are shown with red circles, green stars, and black squares (white stars). The threshold current is marked with the vertical dotted line.

rate is insufficient to capture the faster phase variations in this range of currents. This can be checked by increasing the sampling rate to 10 GSa/s as shown in Fig. 6 with the white stars symbols. These represent the values of D_τ obtained for $I \leq I_{th}$ (the value obtained at $I = 13.4$ mA has also been included to check the convergence with the results obtained for 2GSa/s). As expected, D_τ increases when I decrease in the region below I_{th}, again reaching a saturation behaviour at 12.4 mA due to the same reason as before. This increase of the diffusion coefficient can be illustrated by comparing the phase noise trajectories obtained with 10 GSa/s, shown in Fig.7, with those obtained with 2GSa/s that were shown in Fig. 3(a). A larger widening of the trajectories appears in Fig. 7. In this way fast enough sampling rate is necessary to capture the broadening of the trajectories.

We now discuss how the diffusion coefficient depends on the bias current. Figure 8 shows this dependence in vertical logarithmic scale. The experimental points are shown with black squares and correspond to D_τ if $I \leq I_{th}$ and D_F if $I > I_{th}$, obtained for 10 GSa/s and 2 GSa/s, respectively. We have chosen the values of D_F because the most fundamental function for evaluating the phase noise is the FM-noise spectrum, since $\sigma_\varphi^2(\tau)$ is derived from $S_F(f)$ [29,32].
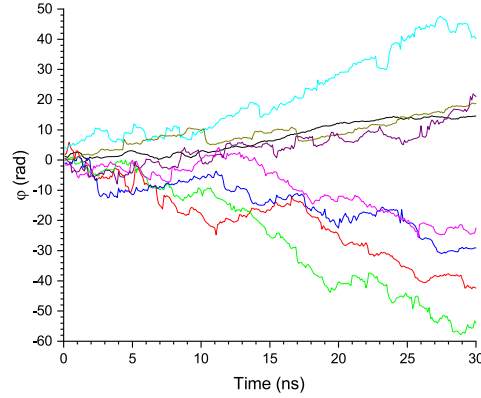
Fig. 7. Phase noise for different temporal trajectories for a bias current of 12.7 mA. In this figure the sampling rate is 10 GSa/s and $T_w = 1 \, \mu$s.
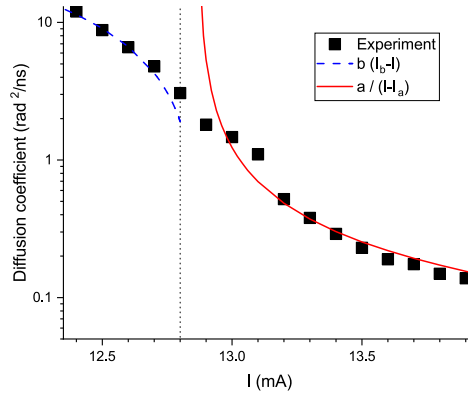

Fig. 8. Diffusion coefficient as a function of the bias current. Experimental values of D_τ (D_F) are plotted with black squares for $I \leq I_{\text{th}}$ ($I > I_{\text{th}}$). Fits of the experimental points to linear and inversely linear relations are shown with dashed and solid lines, respectively.

The diffusion coefficient decreases when increasing I with a small shoulder appearing slightly above I_{th}, between 12.9 mA and 13.2 mA. Similar shoulders have been observed in a directly related quantity, the spectral linewidth, $\Delta \nu$, both in experiments and theory [45–47]. The appearance of this characteristic is related to the non-zero value of the linewidth enhancement factor, α. Moreover, shoulders can develop into local maxima as α increases [45]. The solution of the Fokker-Planck equation (FPE) associated to the laser diode around threshold has described well the observed experimental results [45–47].

Solving the FPE to obtain phase statistics could accurately describe the experimental results shown in Fig. 8, but that is beyond the scope of this work. As an alternative description we will use approximate analytical expressions valid close to threshold, but not exactly at threshold, to get the approximate dependence of D_φ on I.

The rate equations that describe the dynamical evolution of the photon number, P, optical phase, ϕ, and carrier number, N are [37]:

$$\frac{dP}{dt} = \left[\frac{G_N(N - N_t)}{1 + \epsilon P} - \frac{1}{\tau_p} \right] P + \beta B N^2 + \sqrt{2\beta B \bar{P} \bar{N}} F_p(t) \qquad (6)$$

$$\frac{d\phi}{dt} = \frac{\alpha}{2}\left[G_N(N - N_t) - \frac{1}{\tau_p}\right] + \sqrt{\frac{\beta B}{2\bar{P}}}\bar{N}F_\phi(t) \tag{7}$$

$$\frac{dN}{dt} = \frac{I}{e} - (AN + BN^2 + CN^3) - \frac{G_N(N - N_t)P}{1 + \epsilon P} \tag{8}$$

where G_N is the differential gain, ϵ is the non-linear gain coefficient, N_t is the carrier number at transparency, τ_p is the photon lifetime, β is the fraction of spontaneous emission coupled into the lasing mode, α is the linewidth enhancement factor, I is the injected current, e is the electron charge, and A, B and C are the non-radiative, spontaneous, and Auger recombination coefficients, respectively. $\bar{N}$ and $\bar{P}$ are the averaged number of carriers and photons, respectively, and $F_p(t)$ and $F_\phi(t)$ are the Langevin noise terms for the photon and carrier number, respectively. The optical phase $\phi(t)$ is written in the reference frame of the optical frequency at the threshold current, ω_{th}, so the relation between $\phi(t)$ and the phase noise $\varphi(t)$ is given by $\varphi(t) = \phi(t) - (\omega_s - \omega_{th})t$ [39].

When $I \lesssim I_{th}$ the solution of the stochastic rate equations gives $\sigma_\varphi^2 = 2D_\varphi t$, where $D_\varphi = \beta B\bar{N}^2/(4\bar{P})$ [37]. Applying the Schawlow-Townes law, $\Delta\nu = \beta B\bar{N}^2/(2\pi\bar{P})$ [36,37], we obtain $D_\varphi = \pi\Delta\nu/2$. $\Delta\nu$ can be expressed in terms the differential carrier lifetime at threshold, τ_n, as $\Delta\nu = \tau_n G_N(I_{th} - I)/(2\pi e)$, where τ_n is obtained as $\tau_n = (A + 2BN_{th} + 3CN_{th}^2)^{-1}$ [38,42]. Substituting this value in the previous expression for D_φ we obtain

$$D_\varphi = \frac{\tau_n G_N}{4e}(I_{th} - I) \quad \text{if } I \lesssim I_{th} \tag{9}$$

If $I>I_{th}$ the solution of the stochastic rate equations gives $\sigma_\varphi^2 = 2D_\varphi t$, where $D_\varphi = \beta BN_{th}^2(1 + \alpha^2)/(4\bar{P})$ [37], where N_{th} is the carrier number at threshold. Applying the modified Schawlow-Townes law, $\Delta\nu = \beta BN_{th}^2(1 + \alpha^2)/(4\pi\bar{P})$ [36,37], we obtain $D_\varphi = \pi\Delta\nu$. Since $\bar{P} = \tau_p(I - I_{th})/e$, we obtain that

$$D_\varphi = \frac{(1 + \alpha^2)e\beta BN_{th}^2}{4\tau_p}\frac{1}{I - I_{th}} \quad \text{if } I>I_{th} \tag{10}$$

Equation (9) and Eq. (10) are approximate expressions that are not valid very close to I_{th} since when $I = I_{th}$ give unreasonable results. In order to check if Eq. (9) gives an approximate description of $D_\varphi = D_\varphi(I)$ when $I \lesssim I_{th}$ we have fitted the points below threshold to a linear relation $D_\varphi = b(I_b - I)$ to obtain that $b = 23.8$ rad^2/(ns mA) and $I_b = 12.88$ mA. Similarly, when $I>I_{th}$ we fit the experimental points to the following relation, $D_\varphi = a/(I - I_a)$ to obtain that $a = 0.16$ rad^{2}mA/ns and $I_a = 12.87$ mA. The two previous fits have been included in Fig. 8 with dashed and solid lines showing that Eq. (9) and Eq. (10) approximately describe the relation between the phase diffusion coefficient and the bias current, providing that I is not too close to I_{th}. The comparison between the experimental values of a and b and those calculated from the previous expressions using the laser physical parameters would strengthen the validation of the analytical model. However, unfortunately we do not know the values of the physical parameters corresponding to the DFB laser of the experiment. In previous works we performed a complete extraction of the physical parameters, but for a different type of single-mode laser (DML, discrete mode laser) [48]. Since we do not know the DFB parameters we have not calculated a and b from the laser parameters. However we think it is interesting to check it and we plan it for future work.

5. Discussion and summary

The discussion of the statistical properties of the optical phase near the threshold is important because phase noise gain-switched QRNGs can operate at faster rates if the off bias current is close to threshold, providing that phase randomisation during turn-off is large enough. Operation close to threshold is also relevant because phase randomisation is expected to increase significantly below the threshold value. The performance of phase noise QRNGs improves

as faster randomisation of the optical phase takes place, that is, with larger values of the phase diffusion coefficient. This coefficient has already a large value at threshold (12.8 mA), around 3 rad^2/ns. Slightly decreasing the current (to 12.4 mA) leads to D_τ=12 rad^2/ns, so going from I_{th} to 0.97 I_{th} increase four times the value of D_τ. In this way the laser slightly below threshold is a good candidate for efficient QRNGs. We have analysed the phase diffusion for a constant value of the bias current. An extension of our method to gain-switching operation, a regime in which high-performance phase noise QRNGs operate, is difficult from an experimental point of view since optical frequency excursions are much higher than available instrumental bandwidths. However, our results can be representative of the phase diffusion in gain-switched QRNGs operating at rates in which the steady state is reached during the low value of the bias current. When this value is around threshold, like in our case, the steady state is reached in a few hundred of ps, meaning that our results can be representative for QRNGs operating at 1 GHz rate or below.

In [39] we performed measurements of the phase diffusion coefficient for another type of single-mode laser, the DML. However, those measurements were restricted to just one value of the bias current, slightly below threshold, showing that the values of D_φ and D_τ coincide, as in this experiment. This was in fact one of our main motivations to choose the DFB for our experiment: to check that qualitative results do not depend on the choice of single-mode laser. We would expect that most of the observed features in our experiment do not rely on the specific type of single-mode laser. However, some qualitative new features could appear in lasers with high values of α: the observed local maximum in the laser linewidth at a certain bias current slightly above the threshold current value [45] could suggest the presence of a local maximum also in the phase diffusion coefficient.

It is well known that the α factor vary continuously with the bias current [49,50]. However we expect that this variation would be small in our experiment because the considered bias current goes from 0.961 I_{th} to 1.086 I_{th}. The variation of the α factor with the current has been measured in a variety of quantum well structures [49,50]. The measured variation of α over ranges like that considered in our experiment is small [49,50], so we expect that considering a constant value of α in our analysis is a reasonable approximation.

In this work we have measured the statistics of the optical phase of the light emitted by a DFB laser. We have focused on the bias current region around the threshold value. In that region we have shown that the phase diffusion coefficient monotonously decreases as bias current is increased with a shoulder shaped appearing for a current slightly above the threshold value. A good agreement has been obtained when using different methods to measure the phase noise. Finally, we have shown that our experimental results are well described by simple analytical expressions based on the Schawlow-Townes laws, providing that the bias current is not too close to the threshold value.

References

1. M. Stipčević and Ç. K. Koç, "True random number generators," in *Open Problems in Mathematics and Computational Science* (Springer, 2014), pp. 275–315.
2. M. Herrero-Collantes and J. C. Garcia-Escartin, "Quantum random number generators," Rev. Mod. Phys. **89**(1), 015004 (2017).
3. V. Mannalatha, S. Mishra, and A. Pathak, "A comprehensive review of quantum random number generators: Concepts, classification and the origin of randomness," Quantum Inf. Process. **22**(12), 439 (2023).
4. O. Alkhazragi, H. Lu, W. Yan, *et al.*, "Semiconductor emitters in entropy sources for quantum random number generation," Ann. Phys. **535**(9), 2300289 (2023).
5. F. Xu, X. Ma, Q. Zhang, *et al.*, "Secure quantum key distribution with realistic devices," Rev. Mod. Phys. **92**(2), 025002 (2020).
6. T. K. Paraïso, R. I. Woodward, D. G. Marangon, *et al.*, "Advanced laser technology for quantum communications (tutorial review)," Adv. Quantum Technol. **4**(10), 2100062 (2021).
7. D. Rusca and N. Gisin, "Quantum cryptography: an overview of quantum key distribution," arXiv (2024).
8. J. G. Rarity, P. Owens, and P. Tapster, "Quantum random-number generation and key sharing," J. Mod. Opt. **41**(12), 2435–2444 (1994).
9. T. Jennewein, U. Achleitner, G. Weihs, *et al.*, "A fast and compact quantum random number generator," Rev. Sci. Instrum. **71**(4), 1675–1680 (2000).
10. C. Gabriel, C. Wittmann, D. Sych, *et al.*, "A generator for unique quantum random numbers based on vacuum states," Nat. Photonics **4**(10), 711–715 (2010).
11. C. Bruynsteen, T. Gehring, C. Lupo, *et al.*, "100-gbit/s integrated quantum random number generator based on vacuum fluctuations," PRX Quantum **4**(1), 010330 (2023).
12. B. Qi, Y.-M. Chi, H.-K. Lo, *et al.*, "High-speed quantum random number generation by measuring phase noise of a single-mode laser," Opt. Lett. **35**(3), 312–314 (2010).
13. F. Raffaelli, P. Sibson, J. E. Kennard, *et al.*, "Generation of random numbers by measuring phase fluctuations from a laser diode with a silicon-on-insulator chip," Opt. Express **26**(16), 19730–19741 (2018).
14. J.-R. Álvarez, S. Sarmiento, J. A. Lázaro, *et al.*, "Random number generation by coherent detection of quantum phase noise," Opt. Express **28**(4), 5538–5547 (2020).
15. J. Li, Z. Huang, C. Yu, *et al.*, "Quantum random number generation based on phase reconstruction," Opt. Express **32**(4), 5056–5071 (2024).
16. Z. Huang, J. Li, Y. Chen, *et al.*, "Hybrid integrated gbps quantum random number generator based on laser phase fluctuation," Opt. Express **33**(5), 11985–11995 (2025).
17. M. Jofre, M. Curty, F. Steinlechner, *et al.*, "True random numbers from amplified quantum vacuum," Opt. Express **19**(21), 20665–20672 (2011).
18. C. Abellán, W. Amaya, M. Jofre, *et al.*, "Ultra-fast quantum randomness generation by accelerated phase diffusion in a pulsed laser diode," Opt. Express **22**(2), 1645–1654 (2014).
19. Z. Yuan, M. Lucamarini, J. Dynes, *et al.*, "Robust random number generation using steady-state emission of gain-switched laser diodes," Appl. Phys. Lett. **104**(26), 261112 (2014).
20. C. Abellan, W. Amaya, D. Domenech, *et al.*, "Quantum entropy source on an inp photonic integrated circuit for random number generation," Optica **3**(9), 989–994 (2016).
21. V. Lovic, D. G. Marangon, M. Lucamarini, *et al.*, "Characterizing phase noise in a gain-switched laser diode for quantum random-number generation," Phys. Rev. Appl. **16**(5), 054012 (2021).
22. R. Shakhovoy, M. Puplauskis, V. Sharoglazova, *et al.*, "Phase randomness in a semiconductor laser: Issue of quantum random-number generation," Phys. Rev. A **107**(1), 012616 (2023).
23. S. Ó Dúill, L. Rodriguez, D. Alvarez-Outerelo, *et al.*, "Operation of an electrical-only-contact photonic integrated chip for quantum random number generation using laser gain-switching," Optics **4**(4), 551–562 (2023).
24. T. Chrysostomidis, I. Roumpos, D. A. Outerelo, *et al.*, "Long term experimental verification of a single chip quantum random number generator fabricated on the inp platform," EPJ Quantum Technol. **10**(1), 5 (2023).
25. D. G. Marangon, P. R. Smith, N. Walk, *et al.*, "A fast and robust quantum random number generator with a self-contained integrated photonic randomness core," Nat. Electron. **7**(5), 396–404 (2024).
26. C. Henry, "Phase noise in semiconductor lasers," J. Lightwave Technol. **4**(3), 298–311 (1986).
27. R. Loudon, *The Quantum Theory of Light* (Oxford University Press, 2000).
28. K. Kikuchi, "Fundamentals of coherent optical fiber communications," J. Lightwave Technol. **34**(1), 157–179 (2015).
29. K. Kikuchi, "Characterization of semiconductor-laser phase noise and estimation of bit-error rate performance with low-speed offline digital coherent receivers," Opt. Express **20**(5), 5291–5302 (2012).
30. J. Geng, C. Spiegelberg, and S. Jiang, "Narrow linewidth fiber laser for 100-km optical frequency domain reflectometry," IEEE Photonics Technol. Lett. **17**(9), 1827–1829 (2005).
31. J. Li, Z. Yu, Z. Du, *et al.*, "Standoff chemical detection using laser absorption spectroscopy: a review," Remote Sens. **12**(17), 2771 (2020).
32. T. Okoshi and K. Kikuchi, *Coherent Optical Fiber Communications*, vol. 4 (Springer Science & Business Media, 1988).
33. M. Lax and W. Louisell, "Quantum noise. xii. density-operator treatment of field and population fluctuations," Phys. Rev. **185**(2), 568–591 (1969).

34. K. Petermann, *Laser Diode Modulation and Noise*, vol. 3 (Springer Science & Business Media, 1991).
35. G. P. Agrawal and N. K. Dutta, *Semiconductor Lasers* (Springer Science & Business Media, 2013).
36. L. A. Coldren, S. W. Corzine, and M. L. Mashanovitch, *Diode Lasers and Photonic Integrated Circuits*, vol. 218 (John Wiley & Sons, 2012).
37. A. Quirce and A. Valle, "Phase diffusion in gain-switched semiconductor lasers for quantum random number generation," Opt. Express **29**(24), 39473–39485 (2021).
38. A. Quirce and A. Valle, "Spontaneous emission rate and phase diffusion in gain-switched laser diodes," Opt. Laser Technol. **150**, 107992 (2022).
39. I. P. de Zulueta and A. Valle, "Theoretical and experimental analysis of phase noise in semiconductor lasers biased below threshold," Journal of Physics: Photonics **7**, 015013 (2025).
40. T. Duthel, G. Clarici, C. R. Fludger, *et al.*, "Laser linewidth estimation by means of coherent detection," IEEE Photonics Technol. Lett. **21**(20), 1568–1570 (2009).
41. L. Bjerkan, A. Royset, L. Hafskjaer, *et al.*, "Measurement of laser parameters for simulation of high-speed fiberoptic systems," J. Lightwave Technol. **14**(5), 839–850 (1996).
42. P. Pérez, A. Valle, I. Noriega, *et al.*, "Measurement of the intrinsic parameters of single-mode vcsels," J. Lightwave Technol. **32**(8), 1601–1607 (2014).
43. A. Valle, "Divergence of the variance of the optical phase in gain-switched semiconductor lasers described by stochastic rate equations," Phys. Rev. Appl. **19**(5), 054005 (2023).
44. K. Igarashi, H. Kiwata, M. Kikuta, *et al.*, "Measurement of laser phase noise for ultra-long period of 0.8 seconds with 800-ps temporal resolution using optical coherent detection with fpga-implemented data acquisition," J. Lightwave Technol. **39**(20), 6539–6546 (2021).
45. Z. Toffano, "Investigation of threshold transition in semiconductor lasers," IEEE J. Sel. Top. Quantum Electron. **3**(2), 485–490 (1997).
46. T. Fordell, Z. Toffano, S. A. M. Lindberg, *et al.*, "A vertical-cavity surface-emitting laser at threshold," IEEE Photonics Technol. Lett. **18**(21), 2263–2265 (2006).
47. T. Fordell and A. M. Lindberg, "Experiments on the linewidth-enhancement factor of a vertical-cavity surface-emitting laser," IEEE J. Quantum Electron. **43**(1), 6–15 (2007).
48. A. Rosado, A. Perez-Serrano, J. M. G. Tijero, *et al.*, "Numerical and experimental analysis of optical frequency comb generation in gain-switched semiconductor lasers," IEEE J. Quantum Electron. **55**(6), 1–12 (2019).
49. J. Stohs, D. J. Bossert, D. J. Gallant, *et al.*, "Gain, refractive index change, and linewidth enhancement factor in broad-area GaAs and InGaAs quantum-well lasers," IEEE J. Quantum Electron. **37**(11), 1449–1459 (2002).
50. D. Rodriguez, I. Esquivias, S. Deubert, *et al.*, "Gain, index variation, and linewidth-enhancement factor in 980-nm quantum-well and quantum-dot lasers," IEEE J. Quantum Electron. **41**(2), 117–126 (2005).